

crowave *Guided Wave Lett.*, Vol. MGW-2, No. 2, Feb. 1992, pp. 49–51.

13. T. Itoh (Ed.), *Numerical Techniques for Microwave and Millimeter-Wave Passive Structures*, Wiley, New York, 1989.
14. T. Itoh and R. Mittra, "A Technique for Computing Dispersion Characteristics of Shielded Microstrip Lines," *IEEE Trans. Microwave Theory Tech.*, Oct. 1974, pp. 896–898.

Received 3-21-95

Microwave and Optical Technology Letters, 9/6, 312–315
© 1995 John Wiley & Sons, Inc.
CCC 0895-2477/95

NUMERICAL DISPERSION IN THE FINITE-ELEMENT METHOD USING TRIANGULAR EDGE ELEMENTS

Gregory S. Warren
USAF Rome Laboratory
RL/ERAS
31 Grenier St.
Hanscom AFB, Massachusetts 01731

Waymond R. Scott, Jr.
School of Electrical and Computer Engineering
Georgia Institute of Technology
Atlanta, Georgia 30332

KEY TERMS

Finite-element method, triangular mesh, dispersion, wave propagation

ABSTRACT

The discretization inherent in the finite-element method results in the numerical dispersion of a propagating wave. The numerical dispersion of a time-harmonic plane wave propagating through an infinite, two-dimensional, finite-element mesh composed of uniform triangular edge elements is investigated in this work. The effects on the numerical dispersion of the propagation direction of the wave, the electrical size of the elements, and the mesh geometry are investigated. The dispersion for the hexagonal mesh geometry is shown to be much smaller and to converge at a quicker rate than the other meshes. The dispersion analysis is validated by numerical examples. © 1995 John Wiley & Sons, Inc.

I. INTRODUCTION

The finite-element method is a popular technique in computational electromagnetics. Two different approaches are commonly used when applying the finite-element method to solve vector field problems. In both techniques, the domain of interest is divided into subdomains or elements. The difference in the two approaches is in the manner in which the field is approximated within the elements. In the nodal element approach, each component of the field is represented by an expansion of scalar basis functions, whereas, in the edge-element approach, the vector field is approximated by an expansion of vector basis functions. The latter technique offers some significant advantages over the former. For one, it does not suffer from spurious or nonphysical solutions for many types of problems, as does the nodal element approach [1]. In addition, boundary conditions are generally easier to impose along conductor edges and material interfaces when the edge elements are used.

Even though the finite-element method has been extensively used, the errors associated with it have not been

thoroughly investigated. A quantification of these errors is important for one to have complete confidence in the numerical solution. One of the most significant errors arises from the inability of the polynomial basis functions to represent the fields exactly within an element. This error is commonly called the discretization error and is present when nodal elements or vector elements are utilized. A wave propagating through a mesh of finite elements will experience numerical dispersion as a result of this error.

Most research into the numerical dispersion of plane waves propagating through finite element meshes has concentrated on meshes composed of nodal elements [2–5]. The research into the numerical dispersion of edge-element meshes is not as extensive. The authors have investigated the numerical dispersion for quadrilateral, edge-element meshes [6]. Monk and Parrott have investigated the numerical dispersion of several types of triangular elements for a finite-element time-domain method for Maxwell's equations. Their method uses a separate mesh to approximate the electric field and the magnetic field [7].

In this work, the numerical dispersion of a time-harmonic plane wave propagating through a number of infinite, two-dimensional, finite-element meshes composed of triangular edge elements is investigated. The numerical dispersion is characterized by a cumulative phase error. The phase error is quantified as a function of the electrical size of the elements, the direction of propagation of the plane wave, and the orientation of the elements. Results are given that can serve as a guide in selecting the appropriate element size and mesh geometry. The phase error for the hexagonal mesh is demonstrated to be significantly smaller and to converge quicker than the phase error for the other meshes. Finally, numerical results that verify the analysis are given.

II. DISPERSION ANALYSIS

In order to quantify the numerical dispersion of the vector finite-element method, consider an infinite, linear, two-dimensional, homogeneous, isotropic, and source-free region. The field in this region is governed by the vector Helmholtz equation:

$$\nabla \times (\nabla \times \mathbf{E}) - k^2 \mathbf{E} = 0, \quad (1)$$

where an $e^{j\omega t}$ time dependence is assumed and $k = \omega\sqrt{\mu\epsilon}$ is the wave number.

It is well known that a plane wave is an exact solution to the vector Helmholtz equation (1). For the plane-wave solution, the field at any point p is related to the field at any other point q by a simple phase factor:

$$\mathbf{E}_q = \mathbf{E}_p e^{-jk\hat{k}\cdot\Delta\mathbf{r}}, \quad (2)$$

where $\hat{k} = \cos\phi\hat{a}_x + \sin\phi\hat{a}_y$ is a unit vector pointing in the direction of propagation and where $\Delta\mathbf{r}$ is the vector from point p to point q .

Now consider dividing the region into an infinite, uniform mesh. The field in this mesh will be governed by a discretized vector Helmholtz equation. A plane wave propagating along the mesh at an angle ϕ is a solution to the discretized vector Helmholtz equation as well. However, the plane wave propagates with a numerical wave number \hat{k} that differs from the analytical wave number k .

Consider the points p and q depicted in the mesh in Figure 1. The relationship between the discretized field at

any point p within an element and any other point q at the same relative position within another element is a simple phase factor [5, 6]:

$$\tilde{\mathbf{E}}_q = \tilde{\mathbf{E}}_p e^{-j\tilde{k}\cdot\Delta\mathbf{r}}, \quad (3)$$

where $\Delta\mathbf{r}$ is the vector from the point p to point q . It should be emphasized that the relationship between the fields at two arbitrarily located points is not as simple. This is in contrast to the ideal field relationship (2), which is true regardless of the relative location of p and q .

The goal in the dispersion analysis is to determine the relationship between the numerical wave number \tilde{k} and the analytical wave number k . This is accomplished by using the relationship given by (3) in conjunction with residual equations for the unknowns which can be obtained from the vector finite-element formulation [6, 8]. A system of nonlinear equations can be obtained, which can be solved to give the numerical wave number when the analytical wave number is known.

The best way to demonstrate the dispersion analysis process is with a simple example. Figure 2(a) shows a local portion of an infinite mesh of two-dimensional, triangular edge elements. The unknowns associated with the mesh in Figure 2(a) are identified as belonging to group A , B , or C in Figure 2(b). Each unknown within a particular group is

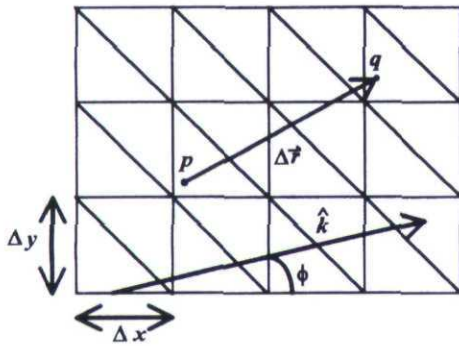


Figure 1 Diagram depicting a plane wave propagating through a portion of an infinite uniform vector finite-element mesh

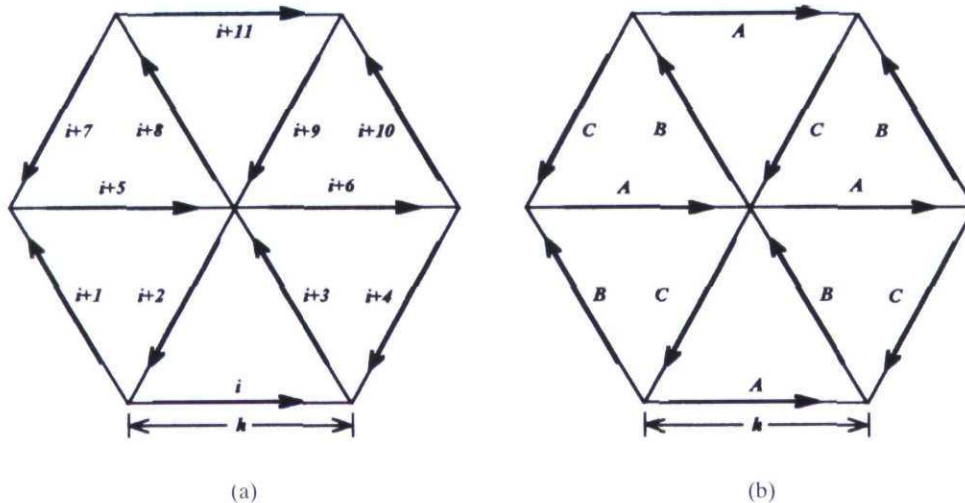


Figure 2 Schematic representation of (a) a local portion of an infinite mesh of triangular edge elements, (b) the groupings of the unknowns in the mesh

located at the same relative position within the mesh. As a result, all the residual equations for the unknowns in that group are equivalent, and only one of these equations is necessary to describe their behavior [6]. Thus, one residual equation from each group is needed to characterize the mesh; three in all for the mesh in Figure 2. The residual equations for the unknowns associated with the basis functions $i + 5$, $i + 3$, and $i + 9$ are chosen to represent their respective groups. Equation (3) is used to express all of the unknowns in a particular group in terms of one of the unknowns in that group. The unknowns in group A are expressed in terms of E_{i+5} , the unknowns in group B in terms of E_{i+3} , and the unknowns in group D in terms of E_{i+9} . Substituting the relationships for all of the unknowns into the residual equations for the unknowns associated with the basis functions $i + 5$, $i + 3$, and $i + 9$ results in the following set of equations:

$$\begin{aligned} R_A = 0 &= 2c_1 + 2c_2[r \cos(k_c/4 + \sqrt{3}k_s/4) \\ &\quad + s \cos(k_c/4 - \sqrt{3}k_s/4)], \\ R_B = 0 &= 2c_1r + 2c_2[\cos(k_c/4 + \sqrt{3}k_s/4) + s \cos(k_c/2)], \\ R_C = 0 &= 2c_1s + 2c_2[\cos(k_c/4 - \sqrt{3}k_s/4) + r \cos(k_c/2)], \end{aligned} \quad (4)$$

where $k_c = \tilde{k}h \cos \phi$, $k_s = \tilde{k}h \sin \phi$, $r = E_{i+3}/E_{i+5}$, $s = E_{i+9}/E_{i+5}$, h is the length of the sides of an element, and the constants c_1 and c_2 are

$$\begin{aligned} c_1 &= \frac{(48 - 5k^2h^2)}{12\sqrt{3}}, \\ c_2 &= \frac{(48 + k^2h^2)}{12\sqrt{3}}. \end{aligned} \quad (5)$$

The three transcendental equations are solved numerically to obtain \tilde{k} as well as r and s .

III. RESULTS

The various meshes investigated in this work are shown in Figure 3. Note that results for the mesh of quadrilateral edge

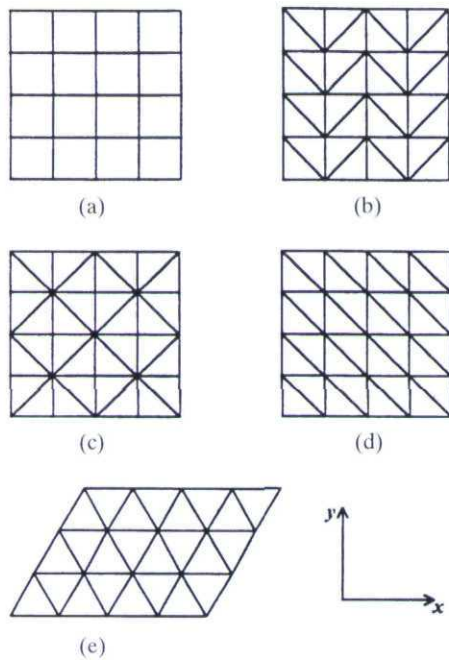


Figure 3 Schematic representations of the uniform, infinite, two-dimensional edge-element meshes: (a) quadrilateral mesh, (b) arrow mesh, (c) diamond mesh, (d) one-directional mesh, and (e) hexagonal mesh

elements are included in this work for comparison [6]. For all of the meshes the length of the shortest side of any element is h . The names for the meshes are given in Figure 3. The numerical wave number \bar{k} for each type of mesh was calculated using the process outlined previously. The resulting phase error, in degrees per wavelength, is defined as

$$\delta_p = 360 \left| \frac{\bar{k} - k}{k} \right|. \quad (6)$$

Figure 4 is a polar graph of the phase error as a function of the angle of propagation ϕ for the one-directional, arrow, diamond, and quadrilateral meshes. Note that the phase errors for the arrow and diamond meshes are almost the same and are within a linewidth of each other in the graph. It can be seen that the phase error for each of the triangular edge element meshes is less than the phase error for the quadrilateral edge element mesh. Figure 5 is a polar graph of the phase error as a function of ϕ for the hexagonal mesh. In both these plots $\lambda/h = 10$. Note the scale change on the graphs; the value of the phase error at the outer edge is indicated on each graph. By comparing Figures 4 and 5 it is quite apparent that the dispersion for the hexagonal mesh is significantly less than that for the other meshes. It can be seen that the phase error for all of the meshes is anisotropic; it varies with the direction of propagation.

For the one-directional, diamond, and arrow meshes, the numerical wave number is sometimes larger than the analytical wave number and sometimes less, depending on ϕ , the angle of propagation of the plane wave through the mesh. The sign of the difference between the two wave numbers, $\bar{k} - k$, is indicated in Figure 4 for each of these meshes. The nulls in the graph of the phase error for the one-directional, arrow, and diamond mesh are the points at which the numerical wave number \bar{k} actually equals the analytical wave num-

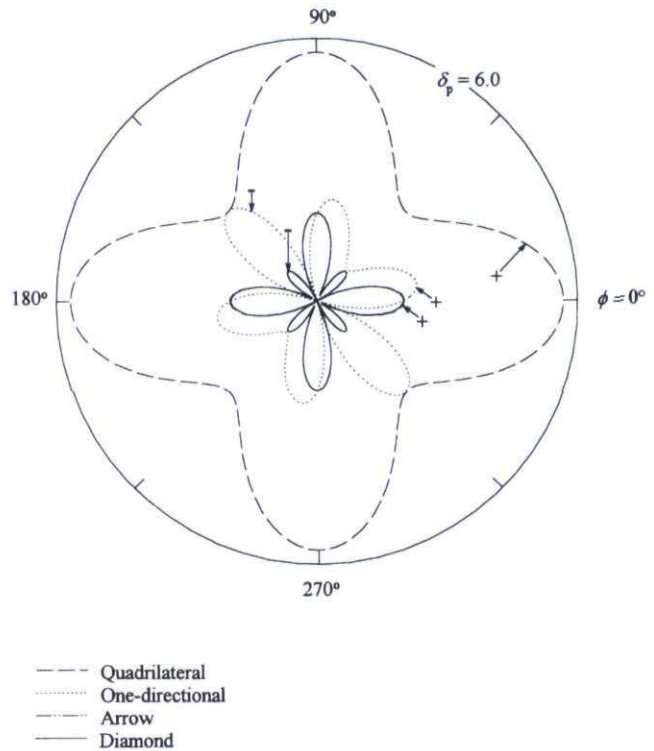


Figure 4 Polar graph of the phase error in degrees per wavelength for the different edge-element meshes as a function of ϕ for $\lambda/h = 10$

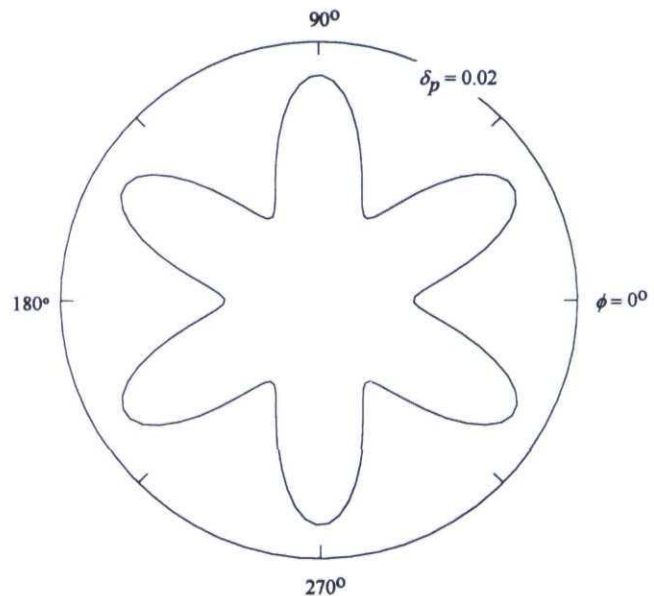


Figure 5 Polar graph of the phase error in degrees per wavelength for the hexagonal mesh as a function of ϕ for $\lambda/h = 10$

ber k . In the case of the quadrilateral and hexagonal meshes, the numerical wave number of a plane wave propagating through either of the meshes is always greater than the analytical wave number, and thus there are no nulls in the graphs of the phase error for these two meshes.

In order to estimate the error in a practical application, one often uses a worst-case scenario. Because the angular dependences of the error for the various meshes differ, it is difficult to use Figures 4 and 5 to get the worst-case error.

Therefore, a worst-case comparison is presented in Figure 6, where the maximum phase error with respect to ϕ is graphed as a function of (λ/h) for each mesh. For all of the meshes except the hexagonal mesh, the error is seen to be proportional to $(\lambda/h)^2$. Thus \bar{k} converges at the rate of $O[(h/\lambda)^2]$ for these meshes. The error for the hexagonal mesh is seen to be proportional to $(\lambda/h)^4$, which indicates that \bar{k} converges at the rate of $O[(h/\lambda)^4]$ for this mesh. Thus, the error for the hexagonal mesh is not only significantly smaller than the error for the other meshes, but it also converges at a much quicker rate.

This high rate of convergence of the phase error for the hexagonal mesh is surprising, since this rate of convergence is usually associated with second-order element meshes [5, 6]. Monk and Parrott [7] observed the same rates of convergence for their edge-constant, finite-element method for Maxwell's equations. The reason for this high rate of convergence is unknown.

IV. NUMERICAL VERIFICATION

A vector finite-element code was written to numerically verify the dispersion analyses and to show that they have relevance for a finite-size mesh. The geometry modeled was an infinitely wide, parallel-plate waveguide of width a and length l with perfectly conducting walls, as in Figure 7. The phase constant of the TM_1 mode in the waveguide is calculated first by the vector finite-element code and then it is predicted using the dispersion relations [6].

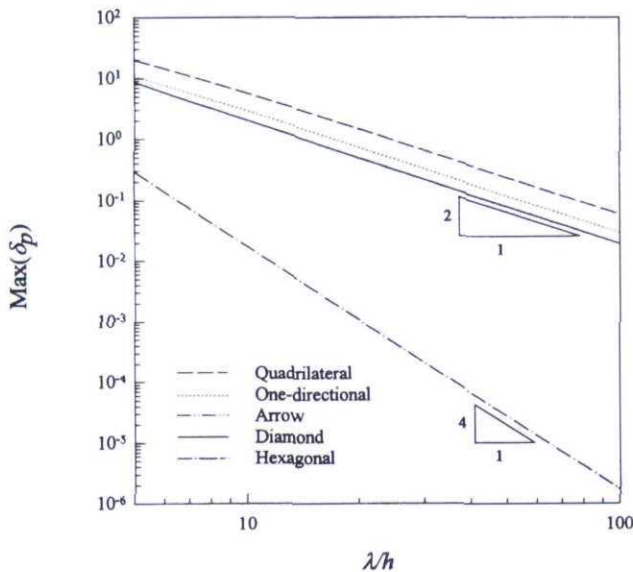


Figure 6 Graph of the maximum phase error with respect to ϕ in degrees per wavelength for the different edge-element meshes as a function of λ/h

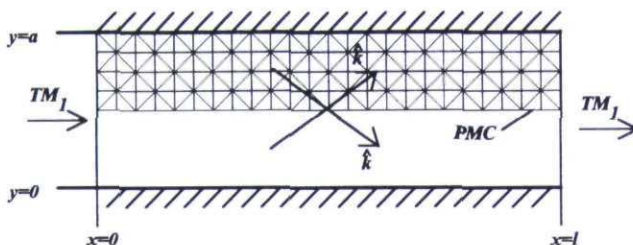


Figure 7 Geometry of the parallel-plate waveguide

The error, δ_β , in the numerical phase constant, $\tilde{\beta}$, in degrees per guide wavelength is

$$\delta_\beta = 360 \left| \frac{\tilde{\beta} - \beta}{\beta} \right|, \quad (7)$$

where β is the phase constant of the TM_1 mode and $\tilde{\beta}$ is the numerical phase constant as determined by first the finite-element code and then predicted by the dispersion relations. Figure 8 and 9 are graphs of the phase constant error as a function of λ/a for the diamond mesh and the hexagonal meshes, respectively. In both graphs, the symbols denote the phase constant error as determined by the finite-element code, and the lines denote the phase constant error using the dispersion analysis. For both types of meshes, the agreement

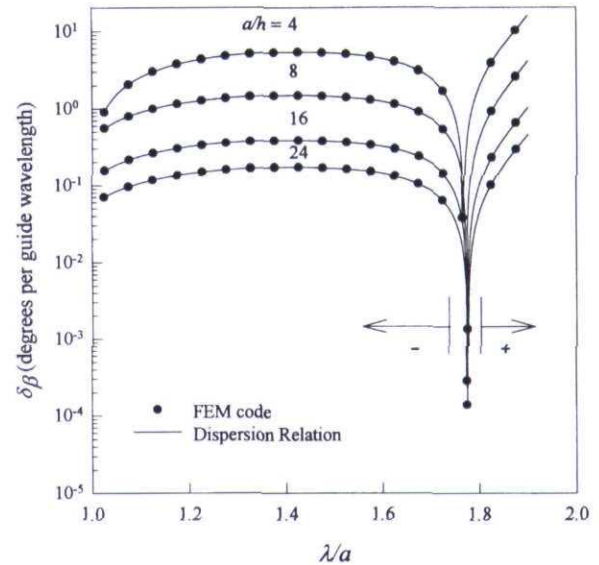


Figure 8 Graph of the error in the phase constant of the parallel-plate waveguide calculated from the finite-element code and from the dispersion relations for the diamond mesh

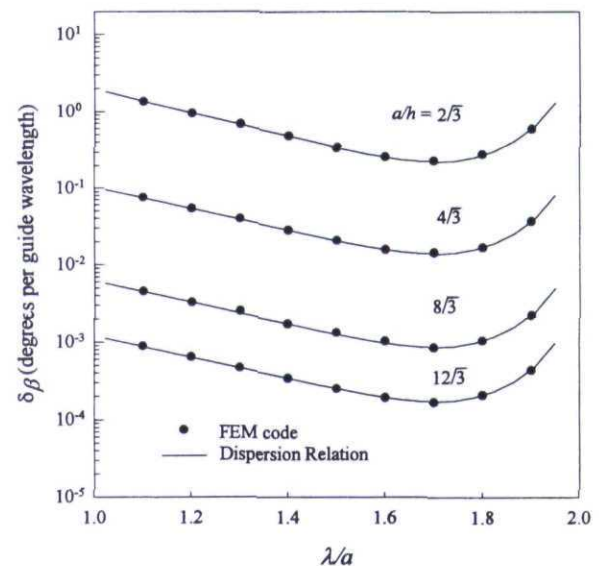


Figure 9 Graph of the error in the phase constant of the parallel-plate waveguide calculated from the finite-element code and from the dispersion relations for the hexagonal mesh

between the results from the code and the dispersion relations is seen to be excellent. Note that the null in the phase constant error in Figure 8 is where $\tilde{\beta}$ is equal to β . The sign of the difference, $\tilde{\beta} - \beta$, is denoted on the graph.

In Figure 10 the phase constant error is presented as a function of a/h with $\lambda/a = 1.5$. The solid line and dashed line are the phase constant error as determined by the dispersion relations for the diamond and hexagonal meshes, respectively. The triangles and the circles are the phase constant error calculated from the finite-element code using the geometry of Figure 7 for the diamond and hexagonal meshes, respectively. The agreement between the results from the finite-element code and the dispersion relations is again seen to be excellent.

From Figures 8–10, it is seen that the hexagonal mesh performs much better than the diamond mesh. In order to see whether a quasihexagonal mesh would maintain this performance, the hexagonal mesh was randomized. This was accomplished by moving the interior vertices of the triangles in the mesh:

$$\begin{aligned} x' &= x + r \cos(\theta), \\ y' &= y + r \sin(\theta), \end{aligned} \quad (8)$$

where x and y are the locations of the vertices of the hexagonal mesh, x' and y' are the locations of the vertices of the quasihexagonal mesh, r is a random number varying uniformly from 0 to $0.1h$, and θ is a random number varying uniformly from 0 to 2π . The finite-element code was run for 10 different quasihexagonal meshes and the rms error for the 10 runs is shown in Figure 10 as the square symbols. From the graph, it is apparent that the performance of the randomized hexagonal meshes is worse than that of the hexagonal mesh, but is better than that of the diamond mesh.

V. CONCLUSION

The phase error that results from the numerical dispersion inherent in the finite-element method when using triangular

edge elements has been investigated. This error is a function of element electrical size, mesh type, and direction of propagation of the plane wave through the mesh. The phase error decreases with an increase in λ/h . The numerical wave number, \tilde{k} , for most edge elements is seen to converge at a rate of $O[(h/\lambda)^2]$. However, the phase error for the hexagonal mesh of edge elements is seen to converge at a rate of $O[(h/\lambda)^4]$. This seems to be a special case that only holds for the ideal, uniform, hexagonal mesh, as was demonstrated by randomizing the hexagonal mesh.

REFERENCES

1. A. R. Pinchuk, C. W. Crowley, and P. P. Silvester, "Spurious Solutions to Vector Diffusion and Wave Field Problems," *IEEE Trans. Magn.*, Vol. MAG-24, Jan. 1988, pp. 158–161.
2. R. Mullen and T. Belytschko, "Dispersion Analysis of Finite Element Semidiscretizations of the Two-Dimensional Wave Equation," *Int. J. Numer. Methods Eng.*, Vol. 18, 1982, pp. 11–29.
3. D. R. Lynch, K. D. Paulsen, and J. W. Strohbehn, "Finite Element Solution of Maxwell's Equations for Hyperthermia Treatment Planning," *J. Comput. Phys.*, Vol. 58, 1985, pp. 246–269.
4. R. Lee and A. Cangellaris, "A Study of Discretization Error in the Finite Element Approximation of Wave Solutions," *IEEE Trans. Antennas Propagation*, Vol. 40, pp. 542–548, May 1992.
5. G. S. Warren and W. R. Scott, Jr., "Numerical Dispersion of Higher-Order Elements in the Scalar Finite-Element Method," *IEEE Trans. Antennas Propagat.*, to be published.
6. G. S. Warren and W. R. Scott, "An Investigation of Numerical Dispersion in the Vector Finite Element Method Using Quadrilateral Elements," *IEEE Trans. Antennas Propagat.*, to be published.
7. P. B. Monk and A. K. Parrott, "A Dispersion Analysis of Finite Element Methods for Maxwell's Equations," *SIAM J. Sci. Comput.*, Vol. 15, No. 4, July 1994, pp. 916–937.
8. J. Jin, *The Finite Element Method in Electromagnetics*, (1st ed.), John Wiley and Sons, New York, 1993.

Received 3-17-95

Microwave and Optical Technology Letters, 9/6, 315–319
© 1995 John Wiley & Sons, Inc.
CCC 0895-2477/95

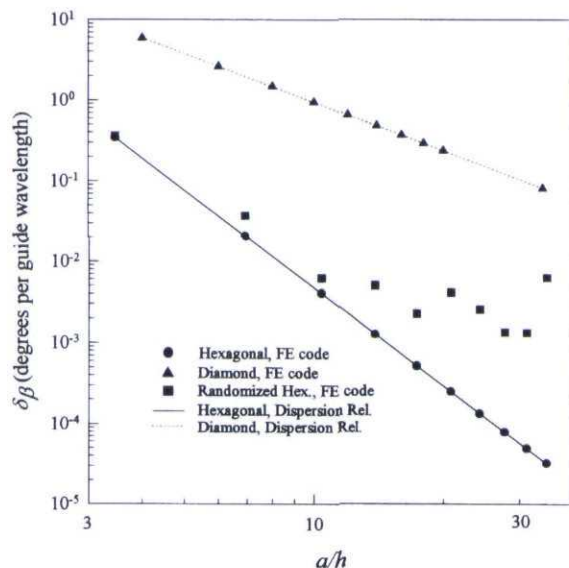


Figure 10 Graph of the error in the phase constant as a function of a/h for the parallel-plate waveguide as determined from the finite-element code for the diamond, hexagonal, and randomized hexagonal meshes, and from the dispersion relations for the diamond and hexagonal meshes

BEAM-PROPAGATION-METHOD ANALYSIS OF A THREE-WAVEGUIDE NONLINEAR DIRECTIONAL COUPLER

Kiyotoshi Yasumoto, Hiroshi Maeda, and Kouichi Nakamura
Department of Computer Science and Communication Engineering
Faculty of Engineering
Kyushu University 36
Fukuoka, 812 Japan

KEY TERMS

Optical waveguides, nonlinear directional coupler, finite-difference beam-propagation method

ABSTRACT

The power-transfer characteristics of a three-waveguide nonlinear directional coupler (NLDC) are investigated with the beam-propagation method based on the finite-difference scheme. The coupler consists of two outer linear waveguides and a center waveguide with a nonlinear Kerrlike medium. It is shown that the three-waveguide NLDC is useful for constructing a power-dependent power divider, a power-dependent

Copyright of Microwave & Optical Technology Letters is the property of Wiley Periodicals, Inc. 2004 and its content may not be copied or emailed to multiple sites or posted to a listserv without the copyright holder's express written permission. However, users may print, download, or email articles for individual use.